

Study of Dynamics of External Neutrons in Reactions ${}^{7,9,11}\text{Li} + {}^{28}\text{Si}$

V.V. Samarin^{1,2}, **M.A. Naumenko**¹

¹Joint Institute for Nuclear Research, 141980 Dubna, Russia

²Dubna State University, 141982 Dubna, Russia

Abstract. This work is devoted to studying light nuclei ${}^{7,9,11}\text{Li}$. The probability density for the ground states of ${}^{7,11}\text{Li}$ nuclei is calculated by Feynman's continual integrals method. The dynamical approach based on the numeric solution of the time-dependent Schrödinger equation is applied to the description of dynamics of outer neutrons in the reaction ${}^{11}\text{Li} + {}^{28}\text{Si}$ and to the calculation of total reaction cross sections.

1 Introduction

The study of nuclear reactions involving neutron-rich weakly bound nuclei makes it possible to obtain information on the structure of the investigated nuclei (clusters, neutron halo, *etc.*) and its manifestation in reactions [1]. It also provides an opportunity for testing various microscopic models. One of the criteria for the limits of applicability and the degree of accuracy of theoretical models is the quantitative agreement between the values of the calculated and the experimentally measured total cross sections of nuclear reactions.

The results of experiments on measuring total cross sections for the ${}^9\text{Li} + {}^{28}\text{Si}$ reaction as a function of energy showed that in the energy range 10 – 20 A MeV the values of the total cross section are much larger than those for the ${}^7\text{Li} + {}^{28}\text{Si}$ reaction [2, 3]. In [2], it was assumed that the reason for the observed behavior was related to the properties of the shell of weakly bound external neutrons and their adiabatic and diabatic rearrangement in the process of collision with the target nucleus. In the ${}^{11}\text{Li}$ nucleus, the external neutrons are even more weakly bound, which determines interest in studying reactions involving this nucleus. In Refs. [4, 5], it was shown experimentally that the total cross sections for reactions involving weakly bound ${}^6\text{He}$ and ${}^{11}\text{Li}$ nuclei can be represented in the form $\sigma_{\text{R}}({}^6\text{He}) \approx \sigma_{\text{R}}({}^4\text{He}) + \sigma_{-2n}({}^6\text{He})$ and $\sigma_{\text{R}}({}^{11}\text{Li}) \approx \sigma_{\text{R}}({}^9\text{Li}) + \sigma_{-2n}({}^{11}\text{Li})$, respectively. In this work, calculations of the total cross sections for the ${}^{11}\text{Li} + {}^{28}\text{Si}$ reaction are based on the model of the ${}^{11}\text{Li}$ nucleus as a system of a ${}^9\text{Li}$ core and two neutrons. The evolution of the wave functions of external neutrons is calculated using a numerical solution of the time-dependent Schrödinger equation. The initial conditions for the wave functions are obtained based on the shell model calculations with the parameters

providing neutron separation energies close to the experimental values as well as results of calculations of probability densities using Feynman's continual integrals method [6–8].

2 Structure of ${}^{7,9,11}\text{Li}$ Nuclei

2.1 Feynman's continual integral method for studying ground states of few-body nuclei

For studying the structure of ${}^{7,11}\text{Li}$ nuclei in the few-body model, we used Feynman's continual integrals method [6, 7]. It provides a mathematically more simple possibility for calculating the energy and the probability density for the ground states of N -body systems compared to other approaches, *e.g.*, hyperspherical harmonics method [7], because it does not require expansion of the wave function into a system of functions. Feynman's continual integral [6, 7] is a propagator – the probability amplitude for a particle to travel from the point q_0 to the point q in a given time t

$$K(q, q_0; t) = \int Dq(t') \exp \left\{ \frac{i}{\hbar} S[q(t')] \right\} = \left\langle q \left| \exp \left(-\frac{i}{\hbar} \hat{H}t \right) \right| q_0 \right\rangle. \quad (1)$$

Here $S[q(t)]$ and \hat{H} are respectively the action and the Hamiltonian of the system, and $Dq(t)$ is the integration measure [8]. For a time-independent potential energy, transition to the imaginary time $t = -i\tau$ yields the propagator $K_E(q, q; \tau)$ with the asymptotic behavior

$$K_E(q, q; \tau) \rightarrow |\Psi_0(q)|^2 \exp \left(-\frac{E_0\tau}{\hbar} \right), \tau \rightarrow \infty \quad (2)$$

or

$$\hbar \ln K_E(q, q; \tau) \rightarrow \hbar |\Psi_0(q)|^2 - E_0\tau, \tau \rightarrow \infty. \quad (3)$$

Expression (3) can be used to obtain the ground-state energy E_0 as the slope of the linear part of the graph representing $\ln K_E(q, q; \tau)$ as a function of τ . The squared modulus of the ground-state wave function $|\Psi_0(q)|^2$ in the points q of the finite region corresponding to finite motion can be determined based on (2) at τ values in the linear part of the graph representing the dependence $\ln K_E(q, q; \tau)$. The approach to calculation of the propagator $K_E(q, q; \tau)$ using Monte Carlo method and NVIDIA CUDA technology was proposed in works [7, 8]. Parallel calculations were performed on the Heterogeneous Cluster of LIT, JINR.

2.2 Structure of ${}^7\text{Li}$ nucleus

In the our model, neutrons (n) and protons (p) in the nuclei interact with each other by nucleon-nucleon potentials with repulsive cores

$$V_{n-n}(r) \equiv V_{p-p}^{(N)}(r) = \sum_{k=1}^3 u'_k \exp(-r^2/b'_k{}^2), \quad (4)$$

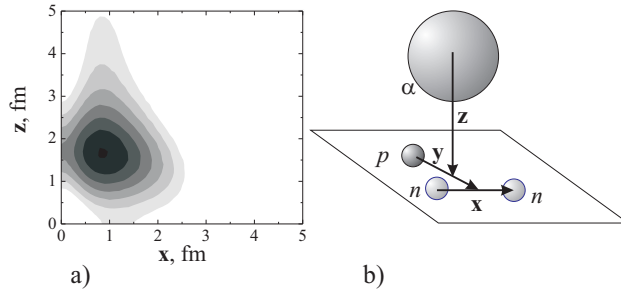


Figure 1. The probability density for the ${}^7\text{Li}$ nucleus in the model $\alpha + p + n + n$ with regular triangle configuration of nucleons and the vectors \mathbf{x} , \mathbf{y} , \mathbf{z} in the Jacobi coordinates; nucleons and α -core are denoted as small and large spheres, respectively. The most probable configuration is $\alpha + \text{triton}$.

$$V_{p-n}(r) = \sum_{k=1}^3 u_k \exp(-r^2/b_k^2). \quad (5)$$

The nuclear part of the α -nucleon potentials used for ${}^6\text{He}$, ${}^6\text{Li}$, ${}^9\text{Be}$ nuclei (see [7, 8]) has a repulsive core for excluding the forbidden (internal) $1s$ state in these nuclei, *e.g.*,

$$V_{\alpha-n}(r) = \sum_{i=1}^3 U_i [1 + \exp((r - R_i)/a_i)]^{-1}. \quad (6)$$

The values of parameters of potentials (4)–(6) are given in Ref. [8]. An example of the probability density for the ground state of ${}^7\text{Li}$ in the 4-body model is shown in Figure 1. The most probable configuration is $\alpha + \text{triton}$, and the neutron separation energies from ${}^7\text{Li}$ nucleus and triton equal to close values: 7.25 MeV and 6.3 MeV, respectively. These values for outer neutrons may be obtained in the shell model of deformed nucleus ${}^7\text{Li}$.

It is well known that the ${}^7\text{Li}$, ${}^9\text{Li}$, ${}^{11}\text{Li}$ nuclei are deformed; the experimental values of the quadrupole deformation parameter β_2 are from -0.9 to -1.5 for ${}^7\text{Li}$, from -0.6 to -0.8 for ${}^9\text{Li}$, -0.6 for ${}^{11}\text{Li}$ [9, 10]. Calculations in the shell model of the deformed nucleus by the method of Ref. [11] with nonspherical Woods–Saxon potential from Ref. [12] provided the energies of the upper occupied levels of the nucleus ${}^7\text{Li}$ approximately equal to the experimental values of the neutron separation energy taken with the opposite sign. The obtained neutron-level diagram is shown in Figure 2a. Two neutrons and two protons at deep lower levels corresponding to the level $1s_{1/2}$ of the spherical nucleus with the projection of the total angular momentum on the axis of symmetry of the nucleus $|m_j| = 1/2$ belong to a nuclear core similar to an α -cluster. In the few-body model, the two external neutrons of the ${}^7\text{Li}$ nucleus on the sublevel with the projection of the total angular momentum on the axis of symmetry of the

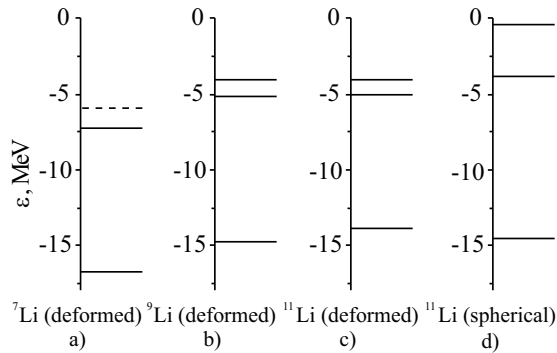


Figure 2. Schemes of neutron levels for the nuclei ^7Li (a), ^9Li (b), and ^{11}Li (c) in the shell model of the deformed nucleus and in the shell model of the spherical nucleus ^{11}Li (d).

nucleus $|m_j| = 3/2$ corresponding to the level $1p_{3/2}$ of the spherical nucleus can be considered quite strongly bound to the triton cluster.

2.3 Structure of ^9Li nucleus

The obtained neutron-level diagram for the ^9Li nucleus is shown in Figure 2b. In the ^9Li nucleus, the neutron separation energy for sublevel $|m_j| = 3/2$ is noticeably lower than in the ^7Li nucleus, and for the higher-lying sublevel with $|m_j| = 1/2$ the separation energy is 4.06 MeV. Thus, for the four external neutrons of the ^9Li nucleus, the bond with the α -cluster core is weakened. In collisions with heavy nuclei, the probability density distribution for these neutrons can change more significantly than for the two external neutrons of the ^7Li nucleus [2].

2.4 Structure of ^{11}Li nucleus

The separation energies of one and two outer neutrons from the ^{11}Li nucleus are very low, 0.40 MeV and 0.37 MeV, respectively, therefore, the ^{11}Li nucleus is considered as a system of a ^9Li -core and two neutrons. An example of the probability density for the ground state of ^{11}Li in this 3-body model is shown in Figure 3. The outer neutrons forming spread weakly-bound dineutron may be considered as independent particles in the shell model.

The level scheme for the neutrons of the deformed ^{11}Li nucleus is shown in Figure 2c. The energies of the sublevels with $|m_j| = 3/2$ and $|m_j| = 1/2$, corresponding to the level $1p_{3/2}$ of the spherical nucleus, turn out to be close. This makes it possible, with sufficient accuracy, to use the spherical shell model for the ^{11}Li nucleus with three filled neutron shells: $1s_{1/2}$ (the α -cluster core shell), $1p_{3/2}$ (the inner skin shell), and $1p_{1/2}$ (the outer halo shell).

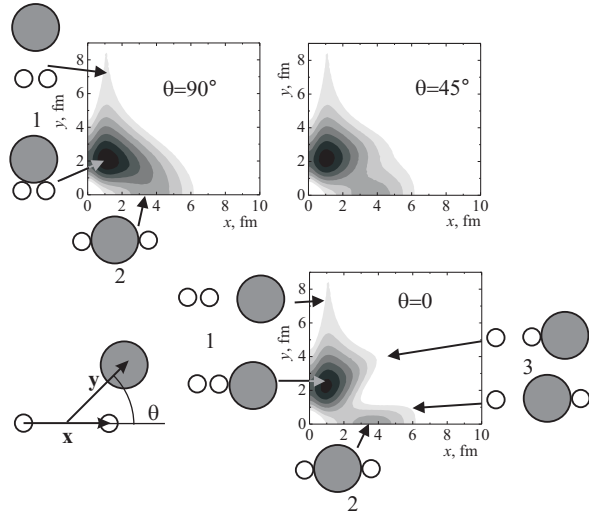


Figure 3. The probability density for the ^{11}Li nucleus (configuration $^9\text{Li} + n + n$) and the vectors in the Jacobi coordinates; neutrons and ^9Li -core are denoted as small empty circles and large filled circles, respectively. The most probable configurations are $^9\text{Li} + \text{dineutron}$ (1) and the cigar configuration (2).

3 Calculation of Total Reaction Cross Sections

As in Refs. [4, 5], we consider two main groups of reaction channels, those that are the consequence of the interaction of the ^9Li -like core of the ^{11}Li nucleus with the ^{28}Si nucleus and the consequence of neutron loss from the outer shell $1p_{1/2}^2$ of the ^{11}Li nucleus. The loss of one neutron (with some probability) leads to a subsequent loss of the second neutron by the unbound ^{10}Li nucleus. The independent probabilities P_{core} of the reaction due to the interaction with the ^9Li -like core of the ^{11}Li nucleus and P_{loss} of the neutron loss from the outer shell can be determined as functions of energy E and the impact parameter b in the semiclassical model: $P_{\text{core}}(b, E)$, $P_{\text{loss}}(b, E)$. The total reaction cross section σ_R can be expressed in terms of these probabilities. The probability of absence of the reaction involving the core is equal to $1 - P_{\text{core}}(b, E)$, the probability of absence of loss at least one neutron is $[1 - P_{\text{loss}}(b, E)]^2$. The probability of the reaction involving the core or due to the loss of a neutron from the outer shell of the ^{11}Li nucleus is equal to

$$P_R(b, E) = 1 - [1 - P_{\text{core}}(b, E)][1 - P_{\text{loss}}(b, E)]^2. \quad (7)$$

In the semiclassical approach, the total cross section for the $^{11}\text{Li} + ^{28}\text{Si}$ reaction is represented by an integral over impact parameters

$$\sigma_{\text{R}} = 2\pi \int_0^{\infty} P_{\text{R}}(b, E) b db. \quad (8)$$

The semiclassical expression for the total cross section of the reaction ${}^9\text{Li} + {}^{28}\text{Si}$

$$\sigma_{\text{R}} = 2\pi \int_0^{\infty} P_{\text{core}}(b, E) b db \quad (9)$$

corresponds to the sum over the orbital angular momenta in the quantum approach

$$\sigma_{\text{R}} = \frac{\pi}{k^2} \sum_{l=0}^{\infty} (2l+1) \tilde{P}_{\text{core}}(l, E) \quad (10)$$

taking into account the relation $l \sim kb$, where k is the modulus of the wave vector. The calculation of the total cross section σ_{R} for the reaction ${}^9\text{Li} + {}^{28}\text{Si}$ and the probability $\tilde{P}_{\text{core}}(l, E)$ in the optical model with the energy-dependent optical potential was performed in Ref. [2] based on the solution of the time-dependent Schrödinger equation for the external neutrons of the ${}^9\text{Li}$ nucleus. The comparison of the results of calculations with the experimental data is shown in Figure 4a. The dependence of the probabilities $P_{\text{core}}(b, E) = \tilde{P}_{\text{core}}(kb, E)$ on b is shown in Figure 4b. An increase in the cross section of the reaction is most noticeable in the energy range at which the relative velocity of the nuclei is close in magnitude to the average velocity of external neutrons in the investigated weakly bound nuclei [2].

For calculation of the probability P_{loss} of neutron loss from the outer shell, we use a time-dependent approach with a quantum description of neutrons in

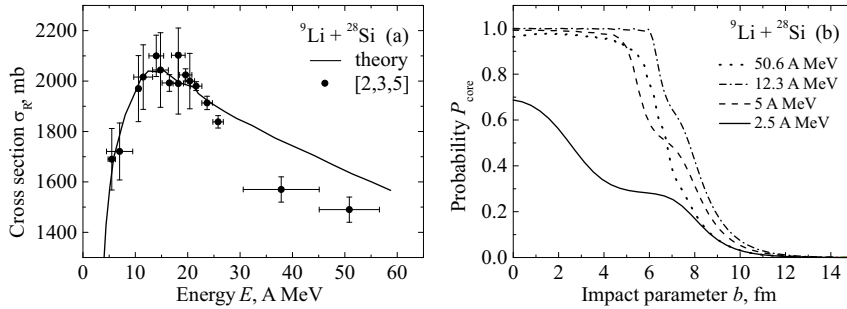


Figure 4. a) The total cross section for the ${}^9\text{Li} + {}^{28}\text{Si}$ reaction: filled circles are the experimental data [2, 3, 5]; the curve is the result of calculations in the optical model with the energy-dependent optical potential [2]. b) Probabilities $P_{\text{core}}(b, E) = \tilde{P}_{\text{core}}(kb, E)$ depending on the impact parameter b for energies 2.5 A MeV (solid line), 5 A MeV (dashed line), 12.3 A MeV (dash-dotted line), 50.6 A MeV (dotted line).

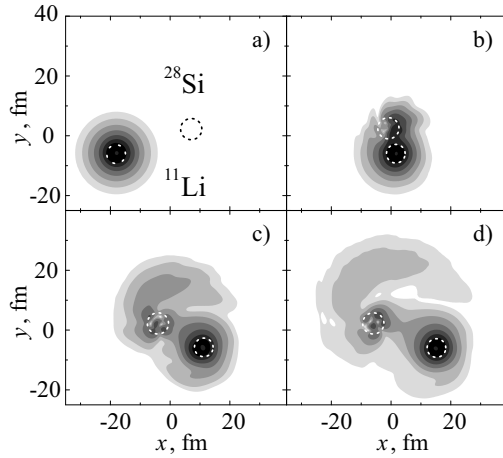


Figure 5. An example of the evolution of the probability density for external neutrons of the ^{11}Li nucleus in the collision with the ^{28}Si nucleus at energy $E = 12.6$ A MeV. The location of the panels a) – d) corresponds to time.

combination with motion of the centers of colliding nuclei along classical trajectories [11, 13, 14]. The two-component spinor wave function $\Psi(\mathbf{r}, t)$ of each of the two independent neutrons with the radius vector \mathbf{r} and the initial state $1p_{1/2}$ was calculated by numerical solution of the time-dependent Schrödinger equation (TDSE) taking into account spin-orbit interaction [2, 15, 16]. The lattice spacing in the TDSE method is 0.15 fm, which is substantially smaller than 0.8 fm in a typical time-dependent Hartree–Fock calculation [17]. The colliding nuclei are enclosed in a box of typical dimensions $90 \times 75 \times 40$ fm³. An example of the evolution of the probability density of external neutrons of the ^{11}Li nucleus in the collision with the ^{28}Si nucleus is shown in Figure 5. It can be seen that at energies ≈ 10 A MeV the external neutrons lost by the ^{11}Li nucleus are transferred to the target nucleus ^{28}Si or leave both nuclei with energy in the continuous spectrum with comparable probabilities P_d and P_c , respectively.

The probabilities $P_d(b, E)$ of neutron transfer to unoccupied bound states of the discrete spectrum in the ^{28}Si nucleus determined in the same way as in Refs. [15, 16] are shown in Figure 6a as functions of the distance of the closest approach $R_{\min}(b, E)$ between the centers of the nuclei. The probabilities P_c of transfer to the states of the continuous spectrum can be determined by integrating the probability density outside the vicinity of the nuclei. As an estimate for P_c , we can use the expression $P_c = CP_{\max}$, where P_{\max} is the maximum value of the probability of neutron presence in the spherical layer D around the ^{28}Si nucleus with boundary radii $r_1 = R_{\text{Si}} + \Delta R_1$ and $r_2 = R_{\text{Si}} + \Delta R_2$; R_{Si} is the radius of the target nucleus ^{28}Si ; C is a variable (adjustable) parameter. It is assumed that the released neutrons initially appear in the layer D in the form of a compact three-dimensional wave packet (see Figure 5) and then gradually

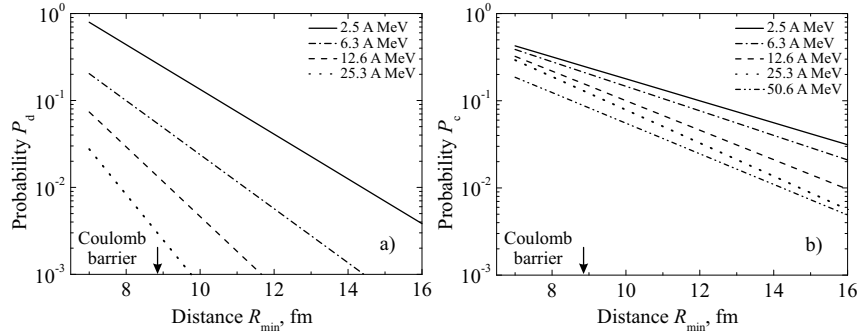


Figure 6. The probabilities of neutron transfer to the unoccupied bound states of the discrete spectrum in the ${}^{28}\text{Si}$ nucleus (a) and the probabilities of transfer to the states of the continuous spectrum with $C = 2$, $\Delta R_1 = 3$ fm, and $\Delta R_2 = 10$ fm (b) for energies 2.5 A MeV (solid line) 6.3 A MeV (dash-dotted line), 12.6 A MeV (dashed line), 25.3 A MeV (dotted line), 50.6 A MeV (dash-dot-dotted line). Arrows indicate the position of the Coulomb barrier.

leave it when the packet spreads. The dependence of the probabilities P_c on $R_{\min}(b, E)$ for $C = 2$, $\Delta R_1 = 3$ fm, and $\Delta R_2 = 10$ fm is shown in Figure 6b.

The probability P_{loss} of neutron loss from the outer shell was determined by the expression

$$P_{\text{loss}}(b, E) = \min \{P_d(b, E) + P_c(b, E), 1\}. \quad (11)$$

The results of calculations of total reaction cross section for the value of the adjustable parameter $C = 2$ for the transition probability to the states of the continuous spectrum are shown in Figure 7. Good agreement with the experimental data is obtained.

In the energy dependence of the total cross section, a sharp maximum is observed at energies near 5 A MeV. On the lower energy side, it is largely due to a sharp increase in the reaction probability P_{core} of the interaction of the target nucleus with the ${}^9\text{Li}$ -like core of the ${}^{11}\text{Li}$ nucleus and an increase in the probability of transfer to the target nucleus of the neutron from the extended halo shell $1p_{1/2}^2$ of the ${}^{11}\text{Li}$ nucleus. A fairly sharp decrease in the total cross section from the high-energy side at $E \approx 10$ A MeV is due to the rapid decrease of the probability of neutron transfer to the target nucleus and the decrease of the reaction probability P_{core} of the interaction of the target nucleus with the ${}^9\text{Li}$ -like core of the ${}^{11}\text{Li}$ nucleus in the region of sharp enhancement of the total cross section for the ${}^9\text{Li} + {}^{28}\text{Si}$ reaction. The energy dependence of the probability P_{core} is due to different interaction time and the influence of the neutron layer (skin) of the inner shell $1p_{3/2}^4$, *i.e.*, the redistribution of an appreciable part of it into the region between the surfaces of the approached nuclei (see Ref. [2]). The probability P_c of transfer to the states of the continuous spectrum from the extended halo shell $1p_{1/2}^2$ changes (decreases) with increasing energy fairly

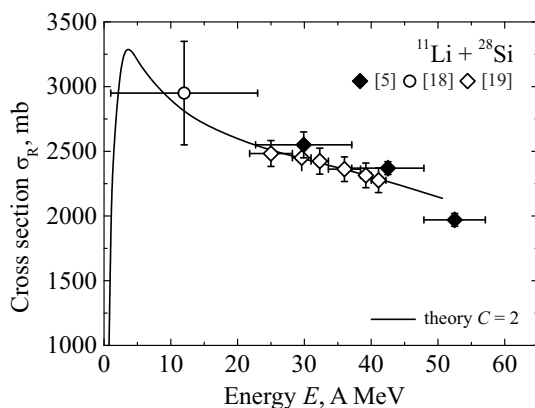


Figure 7. The total cross section for the $^{11}\text{Li} + ^{28}\text{Si}$ reaction: symbols are experimental data [5, 18, 19], curves are the results of calculations for the value of the adjustable parameter $C = 2$ (solid curve) with the probability P_c of transition to the states of the continuous spectrum.

smoothly. This is the reason for the enhancement of the total cross section for the reaction $^{11}\text{Li} + ^{28}\text{Si}$ in comparison with the $^9\text{Li} + ^{28}\text{Si}$ and $^7\text{Li} + ^{28}\text{Si}$ reactions.

4 Conclusions

The experimental data on the total cross sections for the $^{7,9,11}\text{Li} + ^{28}\text{Si}$ reactions have been compared with theoretical calculations. The total cross sections for the $^{11}\text{Li} + ^{28}\text{Si}$ reaction have been calculated based on the numerical solution of the time-dependent Schrödinger equation for the external weakly bound neutrons of the projectile nucleus ^{11}Li . The time-dependent model proposed in the work shows that the sharp maximum in the total cross section is due to the processes of neutron transfer from the external halo shell to the target nucleus and the redistribution of the appreciable part of the inner skin shell into the region between the surfaces of the approached nuclei. Such an increase in the cross section of the reaction is most noticeable in the energy range at which the relative velocity of the nuclei is close in magnitude to the average velocity of external neutrons in the investigated weakly bound nuclei. The enhancement of the cross section for the $^{11}\text{Li} + ^{28}\text{Si}$ reaction compared to those for the $^9\text{Li} + ^{28}\text{Si}$ and $^7\text{Li} + ^{28}\text{Si}$ reactions in the entire energy range (up to 50 A MeV) is due to neutron transfer from the extended halo shell to the states of the continuous spectrum. The calculated total reaction cross sections are in good agreement with the experimental data.

Acknowledgements

The work was supported by the Russian Science Foundation, grant No. 17-12-01170.

References

- [1] Yu.E. Penionzhkevich, *Phys. Atom. Nucl.* **74** (2011) 1615-1622.
- [2] Yu.E. Penionzhkevich, Yu.G. Sobolev, V.V. Samarin, and M.A. Naumenko, *Phys. Atom. Nucl.* **80** (2017) 928-941.
- [3] Yu.G. Sobolev, Yu.E. Penionzhkevich, D. Aznabaev, E.V. Zemlyanaya, *et al.*, *Phys. Part. Nucl.* **48** (2017) 922-926.
- [4] I. Tanihata, D. Hirata, T. Kobayashi, S. Shimoura, K. Sugimoto, and H. Toki, *Phys. Lett. B* **289** (1992) 261-266.
- [5] R.E. Warner, R.A. Patty, P.M. Voyles, A. Nadasen, *et al.*, *Phys. Rev. C* **54** (1996) 1700-1709.
- [6] R.P. Feynman and A.R. Hibbs, *Quantum Mechanics and Path Integrals*. McGraw-Hill, New York (1965).
- [7] V.V. Samarin, *Nuclear Theory* **36**, Heron Press, Sofia (2017) 233-243.
- [8] V.V. Samarin and M. A. Naumenko *Phys. Atom. Nucl.* **80** (2017) 877-889.
- [9] V.I. Zagrebaev, A.S. Denikin, A.V. Karpov, A.P. Alekseev, M.A. Naumenko, V.A. Rachkov, V.V. Samarin, and V.V. Saiko, *NRV Web Knowledge Base on Low-Energy Nuclear Physics* [online knowledge base], URL: <http://nrv.jinr.ru/> [cited 27 September 2018].
- [10] *Centre for Photonuclear Experiments Data*, URL: <http://cdfc.sinp.msu.ru/> [cited 27 September 2018].
- [11] V.V. Samarin, *Phys. Atom. Nucl.* **78** (2015) 128-141.
- [12] V.I. Zagrebaev and V.V. Samarin, *Phys. Atom. Nucl.* **67** (2004) 1462-1477.
- [13] V. Samarin, *EPJ Web Conf.* **86** (2015) 00040.
- [14] V.I. Zagrebaev, V.V. Samarin, and W. Greiner, *Phys. Rev. C* **75** (2007) 035809.
- [15] M.A. Naumenko, V.V. Samarin, Yu.E. Penionzhkevich, and N.K. Skobelev, *Bull. Russ. Acad. Sci.: Phys.* **80** (2016) 264-272.
- [16] M.A. Naumenko, V.V. Samarin, Yu.E. Penionzhkevich, and N.K. Skobelev, *Bull. Russ. Acad. Sci.: Phys.* **81** (2017) 710-716.
- [17] C. Golabek and C. Simenel, *Phys. Rev. Lett.* **103** (2009) 042701.
- [18] A.C.C. Villari, W. Mittig, E. Plagnol, Y. Schutz, *et al.*, *Phys. Lett. B* **268** (1991) 345-350 .
- [19] Li Chen, Ye Yan-Lin, Zhan Wen-Long, Xiao Guo-Qing, *et al.*, *High Energy Physics and Nuclear Physics* **31** (2007) 1102-1105.